ACSNANO

www.acsnano.org

ARTICLE

# Fully Printed Halide Perovskite Light-Emitting Diodes with Silver Nanowire Electrodes

Sri Ganesh R. Bade,[†] Junqiang Li,[†] Xin Shan,[†] Yichuan Ling,[‡] Yu Tian,[⊥] Tristan Dilbeck,[∥] Tiglet Besara,[#] Thomas Geske,[†,⊥] Hanwei Gao,[‡,⊥] Biwu Ma,[§,∥,⊥] Kenneth Hanson,[∥,⊥] Theo Siegrist,[§,⊥,#] Chengying Xu,[⊗] and Zhibin Yu*[,†,⊥]

[†]Department of Industrial and Manufacturing Engineering, High Performance Materials Institute, [§]Department of Chemical and Biomedical Engineering, [#]National High Magnetic Field Laboratory, and [⊗]Department of Mechanical Engineering, Florida State University, Tallahassee Florida 32310, United States

[‡]Department of Physics, [∥]Department of Chemistry and Biochemistry, and [⊥]Materials Science and Engineering, Florida State University, Tallahassee Florida 32306, United States

Supporting Information

**ABSTRACT:** **Printed organometal halide perovskite light-emitting diodes (LEDs) are reported that have indium tin oxide (ITO) or carbon nanotubes (CNTs) as the transparent anode, a printed composite film consisting of methylammonium lead tribromide (Br-Pero) and poly(ethylene oxide) (PEO) as the emissive layer, and printed silver nanowires as the cathode. The fabrication can be carried out in ambient air without humidity control. The devices on ITO/glass have a low turn-on voltage of 2.6 V, a maximum luminance intensity of 21014 cd $m^{-2}$, and a maximum external quantum efficiency (EQE) of 1.1%, surpassing previous reported perovskite LEDs. The devices on CNTs/polymer were able to be strained to 5 mm radius of curvature without affecting device properties.**

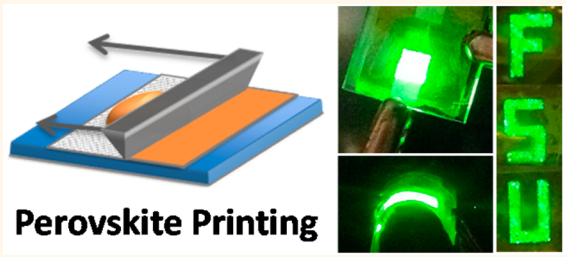


**KEYWORDS:** *halide perovskites, printed electronics, light-emitting diodes, composites, flexible electronics, moisture*

Organometal halide perovskites (Peros) are known to have astounding optoelectronic properties, and their utilization in the fields of solar cells and light-emitting diodes (LEDs) has been well acclaimed in recent years.[1−3] They offer the advantage of high efficiencies, low processing temperatures, cost-effectiveness, and scalable fabrication. For Pero solar cells, the highest power conversion efficiency has reached about 20%, which approaches the best efficiencies of copper indium gallium selenide and cadmium telluride based thin film solar cells.[4,5] Pero LEDs that emit red, green, and blue colors have also been demonstrated.[6−9] With continuous efforts to improve device efficiency and operational stability,[10−15] the next challenge is to develop Pero solar cells and LEDs using a scalable printing technique to realize the promise of large-scale, low-cost devices.[16−19]

In Pero solar cells or LEDs a multilayer device architecture is commonly used that includes the Pero layer, an electron transportation layer (ETL) to facilitate electron collection or injection across the Pero/cathode interface, and a hole transportation layer (HTL) to enhance hole collection or injection at the Pero/anode side. Such a multilayer approach has been shown to benefit the device performance; however, fabrication becomes more complex, requiring the use of orthogonal solvents and usually results in an air-sensitive ETL detrimental to the printing processes. We have shown that a single layer of poly(ethylene oxide) (PEO) and Pero composite thin film sandwiched between an indium tin oxide (ITO) anode and a gold (or an indium/gallium eutectic alloy) cathode can generate efficient electroluminescence without an ETL or a HTL.[20] Such a simplified single-layer device architecture and the use of a high work function cathode are both desirable for printable Pero devices that can be fabricated in ambient conditions.

In this work, we report the first printed Pero LEDs on both rigid ITO/glass and flexible carbon nanotubes (CNTs)/polymer substrates. The devices had ITO or CNTs as the transparent anode, a printed composite film consisting of Br-Pero and PEO as the emissive layer, and printed silver nanowires as the cathode. The printing process can be carried out in ambient air without deliberate humidity control, and it was found that printing the PEO/Br-Pero in air could actually improve its photoluminescence properties. On average, a 256% enhancement in luminous efficiency and a 484% enhancement in maximum luminance intensity ($L_{max}$) were observed in the

Received: November 27, 2015
Accepted: December 29, 2015
Published: December 29, 2015




DOI: 10.1021/acsnano.5b07506
*ACS Nano* 2016, 10, 1795−1801

Pero LEDs that were printed in ambient air compared to those printed in a dry nitrogen atmosphere. The best performing device printed on an ITO/glass substrate possessed a low turn-on voltage of 2.6 V (defined at 1 cd $m^{-2}$), an $L_{max}$ of 21,014 cd $m^{-2}$, and maximum external quantum efficiency (EQE) of 1.1%. Such results represent a new progress over all existing Pero LEDs in the literature that used a multilayer device structure, a spin-coated Pero thin film, and a vacuum-evaporated metal electrode.[3,7,8,21,22] Devices on CNTs/polymer substrates turned on at 2.6 V, with an $L_{max}$ of 360 cd $m^{-2}$ and maximum EQE of 0.14%. Despite the lower performance, the CNT electrode allowed for considerable bending to a radius of curvature of 5 mm without affecting the device properties.

## RESULTS AND DISCUSSION

The printed LEDs were fabricated according to the schematic in Figure 1a. A mixed solution of PEO and Br-Pero in dimethylformamide (DMF) was deposited onto a cleaned ITO/glass or CNTs/polymer substrate. The solution was then spread uniformly using a blade and annealed at 80 °C in air for 5 min to allow the solvent to evaporate completely. A contact mask made of Kapton film was used to define the size and pattern of the active area. Silver nanowires (AgNWs) dispersed in 2-propanol (IPA) were then dropped and spread with another blade. After 1 min of baking at 80 °C in air to evaporate the IPA solvent, the Kapton mask was removed and the device was tested. The LEDs had a lighting area of 3 mm by 3 mm unless otherwise noted. Images of an as-prepared LED device on ITO/glass are shown in Figure 1b (from the AgNW cathode side) and Figure 1c (from the ITO anode side). These photos indicate that both the printed PEO/Br-Pero composite film and the printed AgNW electrode are uniformly dispersed.

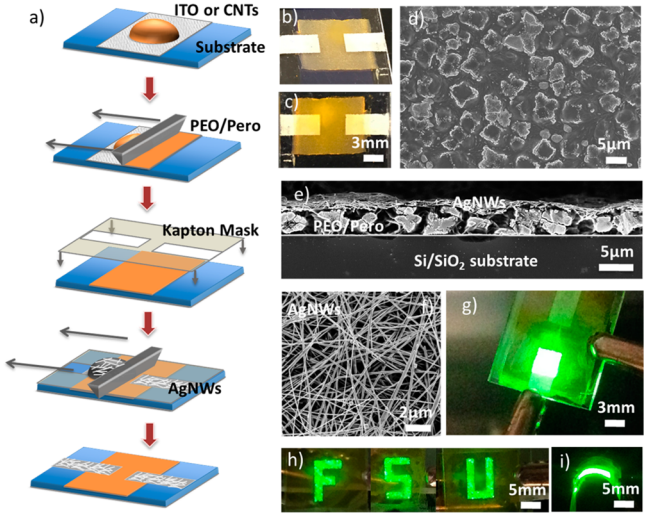


**Figure 1. (a) Schematic showing the fabrication of printed Pero LEDs. (b) Photos of an as-prepared LED device on ITO/glass from the AgNW cathode side and (c) from the ITO anode side. (d) Top view SEM image of the PEO/Br-Pero composite film (0.75:1) and (e) cross-sectional SEM image of the PEO/Br-Pero (0.75:1) emissive layer and AgNW double layer printed onto a silicon/silicon dioxide wafer. f) A SEM top view image of the AgNW electrode. (g) Lit LED on ITO/glass at 4 V. The device emitted green light with ~2400 cd $m^{-2}$ luminance intensity. (h) Displayed "FSU" characters with printed Pero LEDs. The devices emitted ~300 cd $m^{-2}$ green light at a 3.2 V bias. (i) Lit device on a CNTs/polymer substrate after being bent to a 5 mm radius of convex curvature. The device emitted ~200 cd $m^{-2}$ green light.**

The optical microscopic images of the printed PEO/Br-Pero films with PEO/Pero weight ratios of 0.5:1, 0.75:1, and 1:1 can be seen in Figure S1 (Supporting Information). The films were printed in ambient air at 25 °C and 70−85% relative humidity. Dendritic Pero crystals of 20−30 μm size were formed at the 0.5:1 composition. The crystals are separated from each other by 10−20 μm, giving ~60% Pero surface coverage. At higher PEO concentrations (0.75:1 and 1:1), the Br-Pero crystals evolved into a cuboid shape and the separation between neighboring crystals decreased markedly. The finest grain size (5 μm) and highest Pero coverage (~90%) were obtained in the 0.75:1 film; thus, this composition was used for the LEDs described below. The morphology of the 0.75:1 film was further examined by scanning electron microscope (SEM), and the results are shown in Figure 1d. The spacing between the Pero crystals has been completely filled with PEO polymer, and the PEO/Br-Pero composite film is continuous and pinhole free. In contrast, only 20−30% surface coverage was obtained when the Pero solution was printed in air without adding PEO (Figure S2). This observation is consistent with previous reports where moisture was found to play an important role in the crystallization of methylammonium lead triiodide (I-Pero) from a solution phase.[23−25] Very poor coverage was consistently seen when the I-Pero was processed above ~50% relative humidity.[19,24] In this regard, the composite approach in our work is advantageous to eliminating the catastrophic effect of high humidity on the compact emissive layer, which is crucial for preventing electrical shortage and achieving a nearly 100% device yield after printing the top AgNW electrode from solution.

A cross-sectional SEM image of the PEO/Br-Pero (0.75:1) emissive layer and AgNW double layer printed onto a silicon/silicon dioxide wafer is shown in Figure 1e, revealing a PEO/Br-Pero composite layer 3−4 μm thick and a conformal AgNW coating about 300 nm thick. The Pero crystals are partially embedded in the polymer matrix with both size and spatial distribution matching the SEM image in Figure 1d. An SEM top view image of the AgNW electrode (Figure 1f) further clarifies a dense network structure of the printed AgNWs on top of the PEO/Br-Pero film, ensuring low series resistance in the LEDs.

A photo of a functional LED with an ITO anode and AgNW cathode under 4 V of applied potential can be seen in Figure 1g. The device emitted uniform green light with 2400 cd $m^{-2}$ luminance intensity. LEDs that displayed "FSU" characters were also fabricated by changing the contact masks for the AgNW printing step. These patterned devices emitted ~300 cd $m^{-2}$ green light at a 3.2 V bias as shown in Figure 1h. Figure 1i shows an operating device on a CNTs/polymer substrate after being bent to a 5 mm radius of convex curvature.

The crystallinity of Pero in the PEO matrix has been further verified by X-ray diffraction (XRD). The film shows the characteristic peaks of Br-Pero (Figure 2a) for the 0.75:1 composite film,[26] confirming the presence of Br-Pero crystals. The peak at 23.3° can be assigned to the PEO in the composite films (Figure S3). The photoluminescence (PL) and absorption spectra of the composite film were measured, and the results are shown in Figure 2b. The peak in the PL spectrum and the sharp transition in the absorption spectrum both appear at a wavelength of 545 nm, consistent with the band gap of the Br-


DOI: 10.1021/acsnano.5b07506
ACS Nano 2016, 10, 1795−1801

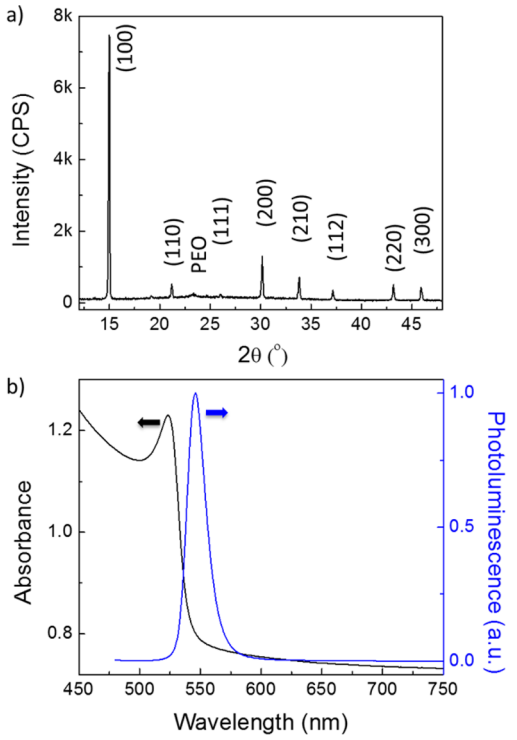


**Figure 2.** (a) X-ray diffraction pattern and (b) absorbance (black) and photoluminescence (blue) spectra of the PEO/Br-Pero composite film (0.75:1).

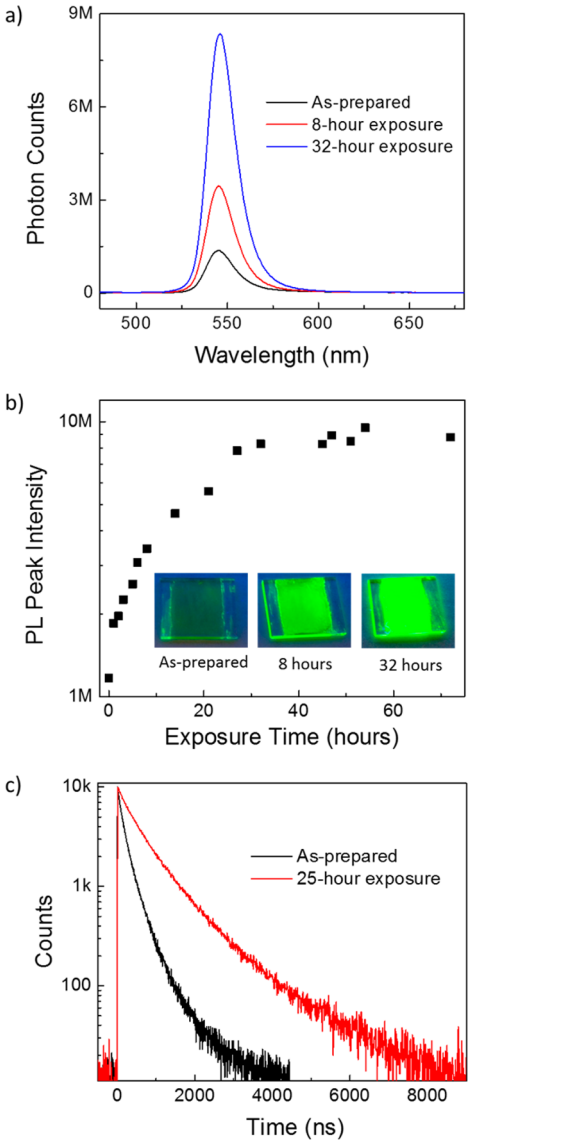


**Figure 3.** (a) PL spectra evolution and (b) peak intensity (at 545 nm) evolution with air exposure time for the PEO/Br-Pero composite film (0.75:1). Insets in (b) show photos of the as-prepared, 8 h and 32 h air-exposure samples under 365 nm UV lamp irradiation. (c) Time-resolved emission traces ($\lambda_{ex}$ = 405 nm, $\lambda_{em}$ = 545 nm) for one as-prepared film (black curve) and after 25 h of exposure to air (red curve).

Pero (2.3 eV). The PL spectrum has a full width at half-maximum of 18 nm.

The stability of the PEO/Br-Pero (0.75:1) composite films was investigated using PL spectroscopy. PL spectra were collected immediately after processing and after exposure to ambient air at 25 °C and 70−85% relative humidity for a specified time. As shown in Figure 3a,b, the peak intensity at 545 nm increased rapidly with exposure time and reached a saturation value at 32 h, with a 612% increase of peak intensity compared to the as-prepared film. After 32 h, the films obtained maximum emission intensity, and the PL intensity remained nearly constant even after an additional 40 h of atmospheric exposure. The insets in Figure 3b are images of the as-prepared, 8 h and 32 h air-exposure samples under 365 nm UV lamp irradiation, suggesting PL intensity enhancement after the air exposure. As a control experiment, another PEO/Br-Pero sample was printed and kept in a nitrogen filled glovebox with both oxygen and moisture concentration at ≤1 ppm. The images in Figure S4 show the PL intensity evolution with time. Compared with humid air, dry nitrogen only slightly increases the PL intensity. The XRD spectrum (Figure S5) and optical images (Figure S6) of the PEO/Br-Pero (0.75:1) film as-prepared and after 20 h air exposure are nearly identical indicating the structural integrity and morphology of the Br-Pero crystals remains unaltered upon exposure to air.

Time-resolved photoluminescence (TrPL) spectroscopy was used to characterize the printed PEO/Br-Pero films (Figure 3c). The photoluminescence decay curves had been fit with a biexponential function eq (Table S1). The air-exposed film had a weighted-average lifetime ($\tau$) of 861 ns, which was much longer than the as-prepared film ($\tau$ = 309 ns). The increased lifetime in the air exposed film may be attributed to a reduction of defect density in the bulk or/and at the interfaces of the Pero crystals, which reduces the nonradiative decay rate and increases the PL intensity.

Humidity-induced PL enhancement in I-Pero thin films has been reported.[24,27] In the work of Eperon *et al.*,[24] such an enhancement was attributed to the partial solvation of the methylammonium component and the self-healing of the perovskite lattice. We postulate that similar behaviors may occur in our Br-Pero films. The PL enhancement of the I-Pero thin films upon moisture exposure was usually accompanied by a morphology and composition deterioration of the I-Pero crystals.[24,27] In contrast, the PEO/Pero composite introduced here is ideal for ambient air printing processes in that it exhibits PL efficiency improvement while maintaining the desired morphology and crystallinity.

Printed LED devices were fabricated and characterized using composite PEO/Br-Pero films with a 0.75:1 weight ratio in the



DOI: 10.1021/acsnano.5b07506
*ACS Nano* 2016, 10, 1795−1801

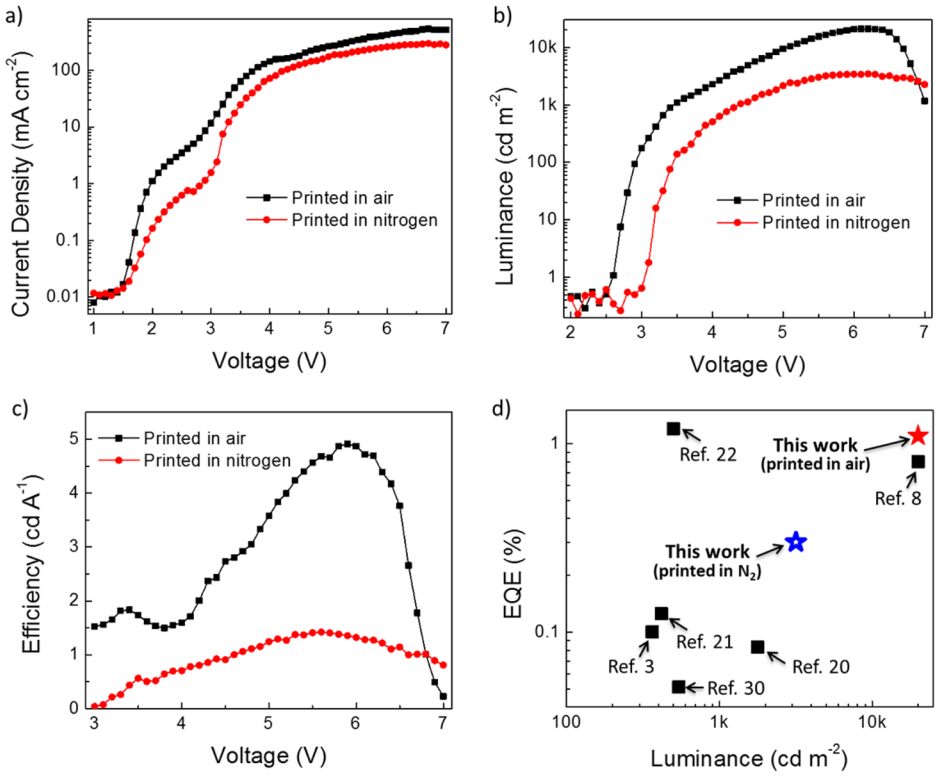


**Figure 4. (a) Current density, (b) luminance, and (c) current efficiency *versus* voltage characteristics of the best performing LEDs printed in air and in a nitrogen-filled glovebox. (d) Comparison of $L_{max}$ and EQEs of our printed Br-Pero LEDs with reported Br-Pero LEDs in literature.**

emissive layer. The films were printed and kept in air (25 °C, 70−85% relative humidity) for 32 h before the top AgNW electrode was printed. As a control experiment, LEDs were also printed in the nitrogen filled glovebox. The current density−voltage ($I-V$), luminance−voltage ($L-V$), and current efficiency−voltage ($E-V$) characteristics of the LEDs are shown in parts a−c, respectively, of Figure 4. Overall, the device printed in air exhibited higher current density than the device printed under nitrogen atmosphere. It is conjectured that air exposure reduced surface defects/traps in the Pero crystals, leading to improved electron/hole injection efficiency across the electrode/Pero interfaces. The device printed in air had a turn-on voltage of 2.6 V, an $L_{max}$ of 21,014 cd m$^{-2}$ (at 6.2 V), a maximum current efficiency ($E_{max}$) of 4.91 cd A$^{-1}$ (at 20000 cd m$^{-2}$ luminance intensity), and an EQE of 1.1%. In contrast, the device printed in the nitrogen glovebox had a turn-on voltage of 3.1 V, an $L_{max}$ of 3,446 cd m$^{-2}$ (at 6.2 V), $E_{max}$ of 1.42 cd A$^{-1}$ (at 3,175 cd m$^{-2}$ luminance intensity), and an EQE of 0.3%, considerably lower than air-processed devices. Statistical summaries for all of the fabricated devices in each group can be found in Figure S7a,b. It is evident that the devices printed in air are superior to the ones printed in the glovebox. On average, a 256% enhancement in EQE and a 484% enhancement in $L_{max}$ was obtained after air exposure, which agrees with the large PL intensity increase in the air-exposed PEO/Br-Pero film.

Turn-on voltages of 3.1 to 4.2 V have been commonly reported by various research groups using a multilayer device structure and a spin-coated Br-Pero thin film as the emissive layer.[3,21,22,28] The much lower turn-on voltages in the air-printed device indicate that very efficient charge carrier injection and transport can be achieved in Pero LEDs that have a relatively thick emissive layer (3−4 $\mu$m) and a very simple single-layer device structure. It is worth noting that the combination of high efficiency and high luminance (an EQE of 1.1% at 20,000 cd m$^{-2}$) of the air-printed device in our work exceeded all reported Pero LEDs in the literature (Figure 4d).[3,7,8,21,22,28−30] For instance, Wang *et al.* reported an EQE of 0.8% at 20000 cd m$^{-2}$ using polyethylenimine-modified zinc oxide as the ETL and poly(9,9-dioctyl-fluorene-*co*-*N*-(4-butylphenyl)diphenylamine)/molybdenum oxide as the HTL in their Br-Pero LEDs;[8] Li *et al.* reported an EQE of 1.2% and a maximum luminance intensity of ∼500 cd m$^{-2}$ using PEDOT/PSS as the HIL, a bromide-Pero/polyimide precursor composite as the emissive layer, and poly(9,9′-dioctylfluorene)/Ca as the ETL in their best Br-Pero LEDs.[22]

Moving further, fully printed and flexible PEO/Br-Pero LEDs were fabricated with a device configuration illustrated in Figure 5a. The transparent anode is composed of single-walled CNTs on polyacrylate substrate (∼200 $\mu$m thick). The PEO/Br-Pero composite layer was printed onto the CNTs/polyacrylate in air, followed by air exposure for 32 h, and then silver nanowires were printed as the cathode electrode. An image of a working device bent to a ∼5 mm radius of convex curvature is shown in Figure 1i, corresponding to applying 2% tensile strain onto the LED device. No luminous degradation was seen after a few bending/releasing cycles (see video 1 and video 2). The $I-V-L$ characteristics of the flexible device are shown in Figure 5b. The device turned on at an applied potential of 2.6 V and obtained an $L_{max}$ of 360 cd m$^{-2}$ at 6.1 V. The $E_{max}$ was 0.6 cd A$^{-1}$ (Figure 5c) with an EQE of 0.14%. The lower luminance intensity and efficiency of the CNT-based devices compared to devices on ITO/glass is presumably due to the higher sheet resistance of the CNT network (500−1000 Ω



DOI: 10.1021/acsnano.5b07506
*ACS Nano* 2016, 10, 1795−1801

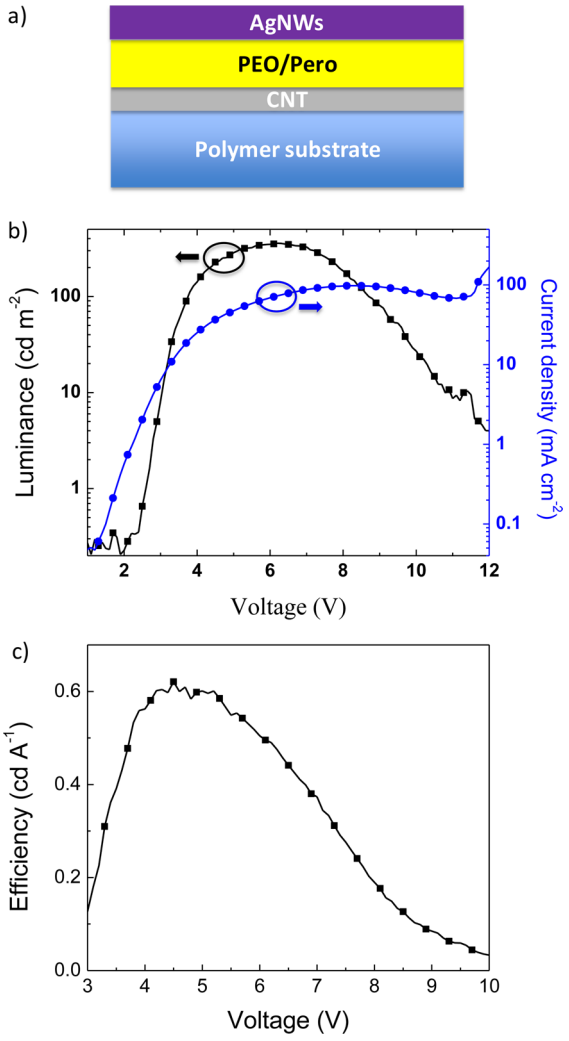


**Figure 5. Fully printed and flexible PEO/Br-Pero LEDs on CNTs/polyacrylate substrates. (a) Schematic showing the device configuration. (b) Current density−voltage−luminance intensity characteristics of one fully printed and flexible LED and (c) its corresponding current efficiency−voltage characteristic.**

square$^{-1}$). Nonetheless, the flexibility of the CNT electrode[31] may be advantageous for roll-to-roll printing of the PEO/Br-Pero layer on plastic substrates.

## CONCLUSION

We demonstrated printed Pero LEDs on both rigid ITO/glass and flexible CNTs/polymer substrates using a composite thin film of PEO and Br-Pero as the light-emitting layer. Printing the PEO/Br-Pero film in an ambient with 70−85% relative humidity results in an increased PL efficiency, 256% enhancement in EQE, and 484% enhancement in luminance intensity over the devices printed in dry environment. The device on an ITO/glass substrate exhibited a low turn-on voltage of 2.6 V, a maximum luminance of 21014 cd m$^{-2}$, and a maximum EQE of 1.1%. All these metrics compare favorably with existing Pero LEDs composed of a multilayer architecture prepared by complex fabrication techniques. Fully printed, highly flexible Pero LEDs on CNTs/polymer substrates were also demonstrated. We believe the material and processing concepts presented in this work could be of great value for future scalable manufacturing of Pero based optoelectronic devices.

## EXPERIMENTAL SECTION

**Materials.** Lead(II) bromide (99.999%), *N*,*N*-dimethylformamide (DMF) (anhydrous, 99.8%), poly(ethylene oxide) ($M_w \approx 5000000$), bisphenol A ethoxylate diacrylate ($M_n \approx 512$), 2,2-dimethoxy-2-phenylacetophenone (DMPA), and single-walled CNT conductive ink (SWeNT VC101 ink) were purchased from Sigma-Aldrich. Polydimethylsiloxane (PDMS) precursors (SYLGARD 182) were purchased from Ellsworth Adhesives. Silver nanowire dispersion in IPA (SLV-NW-90) was purchased from Blue Nano, Inc. The nanowires have an average diameter of 90 nm and length ∼25 μm. The $CH_3NH_3Br$ was purchased from "1-Material Inc." All materials were used as received.

**Static PL and TrPL Measurements.** Static PL spectra were collected at room temperature on a Horiba Jobin Yvon FluoroMax-4 Fluorometer. The excitation wavelength was fixed at 460 nm. The emission spectra from 480 to 780 nm were collected with an integration time of 0.1 s. TrPL data were collected at room temperature using an Edinburgh FLS980 spectrometer. The dynamics of emission decay were monitored by using the FLS980s time-correlated single-photon counting capability (1024 channels; 10 μs window) with data collection for 10,000 counts. Excitation was provided by an Edinburgh EPL-405 ps pulsed diode laser (405.2 nm, 80 ps fwhm) operated at 1 MHz.

**LED Fabrication on ITO/Glass.** The Br-Pero precursor solution was prepared by dissolving $PbBr_2$ and $CH_3NH_3Br$ with a 1:1.5 molar ratio in anhydrous DMF to give a concentration of ∼500 mg mL$^{-1}$. PEO was dissolved in DMF to give a concentration of 10 mg mL$^{-1}$. The perovskite precursor and PEO solutions were then mixed with the desired ratio. All of the solutions were stirred for 30 min at 70 °C before use. The ITO/glass substrates (10 Ω square$^{-1}$, 16 mm × 18 mm size) were cleaned with detergent water, sonicated for 10 min each in acetone, IPA, and distilled water, and then blow dried with nitrogen. Cleaned ITO/glass substrates were treated with oxygen plasma at 100 W power for 3 min. Composite solution (40 μL) was dropped onto the ITO/glass substrate, spread uniformly with a blade, and then dried at 80 °C for 5 min on a hot plate. Kapton tape was cut into the desired shape and dimensions using a laser cutting machine which served as a mask and was applied onto the composite film. A 4 μL portion of silver nanowire suspension (50 mg mL$^{-1}$ in IPA) was dropped onto the electrode area defined by the Kapton mask and spread uniformly using another blade. The devices were then annealed at 80 °C for 1 min before test. The sheet resistance of the printed silver nanowires was about 2−5 Ω square$^{-1}$. Device testing was done inside a nitrogen-filled glovebox with both nitrogen and oxygen concentration at ∼1 ppm.

**CNTs/Polyacrylate Electrode Fabrication.** The single-walled CNT conductive ink was printed onto a cured PDMS substrate using a Meyer rod and dried at 100 °C for 10 min. Photocurable monomers (bisphenol A ethoxylate diacrylate) mixing with 1 wt % of a photoinitiator (DMPA) were applied onto the CNTs/PDMS. The monomers were subjected to UV irradiation and cured into a solid polyacrylate film. By this process, the CNTs became attached to the polyacrylate which was then peeled off from the PDMS. The resistance of the CNT coating remained unchanged after the peeling process. The CNTs on polyacrylate (500−1000 Ω square$^{-1}$) sheet resistance and 60−70% transmittance at 550 nm) serves as the electrode/substrate for the fully printable LEDs.

**LED Measurement.** Current density−voltage and luminance−voltage characteristics were measured with a Keithley 2400 source meter and a silicon photodiode. The silicon photodiode was further calibrated by a photo research PR-655 spectroradiometer.

## ASSOCIATED CONTENT

### Supporting Information

The Supporting Information is available free of charge on the ACS Publications website at DOI: 10.1021/acsnano.5b07506.

Supplemental figures and a table of average lifetimes for perovskites (PDF)



DOI: 10.1021/acsnano.5b07506
ACS Nano 2016, 10, 1795−1801

(MPG)
(MPG)

## AUTHOR INFORMATION


### Corresponding Author

*E-mail: zyu@fsu.edu.


### Notes

The authors declare no competing financial interest.

## ACKNOWLEDGMENTS

We are thankful for the financial support from National Science Foundation under Awards ECCS- 1549888 (program manager Nadia El-Masry). We also thank Dr. Bert van de Burgt for assisting PL measurements at the Materials Characterization Laboratory of FSU.

## REFERENCES


(1) Stranks, S. D.; Snaith, H. J. Metal-Halide Perovskites for Photovoltaic and Light-Emitting Devices. *Nat. Nanotechnol.* **2015**, *10*, 391−402.

(2) Lee, M. M.; Teuscher, J.; Miyasaka, T.; Murakami, T. N.; Snaith, H. J. Efficient Hybrid Solar Cells Based on Meso-Superstructured Organometal Halide Perovskites. *Science* **2012**, *338*, 643−647.

(3) Tan, Z.-K.; Moghaddam, R. S.; Lai, M. L.; Docampo, P.; Higler, R.; Deschler, F.; Price, M.; Sadhanala, A.; Pazos, L. M.; Credgington, D.; Hanusch, F.; Bein, T.; Snaith, H. J.; Friend, R. H. Bright Light-Emitting Diodes Based on Organometal Halide Perovskite. *Nat. Nanotechnol.* **2014**, *9*, 687−692.

(4) Jeon, N. J.; Noh, J. H.; Yang, W. S.; Kim, Y. C.; Ryu, S.; Seo, J.; Seok, S. I. Compositional Engineering of Perovskite Materials for High-Performance Solar Cells. *Nature* **2015**, *517*, 476−480.

(5) Zhou, H.; Chen, Q.; Li, G.; Luo, S.; Song, T.; Duan, H.-S.; Hong, Z.; You, J.; Liu, Y.; Yang, Y. Interface Engineering of Highly Efficient Perovskite Solar Cells. *Science* **2014**, *345*, 542−546.

(6) Jaramillo-Quintero, O. A.; Sanchez, R. S.; Rincon, M.; Mora-Sero, I. Bright Visible-Infrared Light Emitting Diodes Based on Hybrid Halide Perovskite with Spiro-OMeTAD as a Hole-Injecting Layer. *J. Phys. Chem. Lett.* **2015**, *6*, 1883−1890.

(7) Sadhanala, A.; Ahmad, S.; Zhao, B.; Giesbrecht, N.; Pearce, P. M.; Deschler, F.; Hoye, R. L. Z.; Gödel, K. C.; Bein, T.; Docampo, P.; Dutton, S. E.; De Volder, M. F. L.; Friend, R. H. Blue-Green Color Tunable Solution Processable Organolead Chloride−Bromide Mixed Halide Perovskites for Optoelectronic Applications. *Nano Lett.* **2015**, *15*, 6095−6101.

(8) Wang, J.; Wang, N.; Jin, Y.; Si, J.; Tan, Z.-K.; Du, H.; Cheng, L.; Dai, X.; Bai, S.; He, H.; Ye, Z.; Lai, M. L.; Friend, R. H.; Huang, W. Interfacial Control Toward Efficient and Low-Voltage Perovskite Light-Emitting Diodes. *Adv. Mater.* **2015**, *27*, 2311−2316.

(9) Gil-Escrig, L.; Longo, G.; Pertegás, A.; Roldán-Carmona, C.; Soriano, A.; Sessolo, M.; Bolink, H. J. Efficient Photovoltaic and Electroluminescent Perovskite Devices. *Chem. Commun.* **2015**, *51*, 569−571.

(10) Jiang, Q.; Rebollar, D.; Gong, J.; Piacentino, E. L.; Zheng, C.; Xu, T. Pseudohalide-Induced Moisture Tolerance in Perovskite CH3NH3Pb(SCN)2I Thin Films. *Angew. Chem., Int. Ed.* **2015**, *54*, 7617−7620.

(11) Zhang, F.; Zhong, H.; Chen, C.; Wu, X.; Hu, X.; Huang, H.; Han, J.; Zou, B.; Dong, Y. Brightly Luminescent and Color-Tunable Colloidal CH3NH3PbX3 (X = Br, I, Cl) Quantum Dots: Potential Alternatives for Display Technology. *ACS Nano* **2015**, *9*, 4533−4542.

(12) Guarnera, S.; Abate, A.; Zhang, W.; Foster, J. M.; Richardson, G.; Petrozza, A.; Snaith, H. J. Improving the Long-Term Stability of Perovskite Solar Cells with a Porous Al2O3 Buffer Layer. *J. Phys. Chem. Lett.* **2015**, *6*, 432−437.

(13) Bailie, C. D.; McGehee, M. D. High-Efficiency Tandem Perovskite Solar Cells. *MRS Bull.* **2015**, *40*, 681−686.

(14) Wu, C.-G.; Chiang, C.-H.; Tseng, Z.-L.; Nazeeruddin, M. K.; Hagfeldt, A.; Grätzel, M. High Efficiency Stable Inverted Perovskite Solar Cells without Current Hysteresis. *Energy Environ. Sci.* **2015**, *8*, 2725−2733.

(15) Hwang, I.; Jeong, I.; Lee, J.; Ko, M. J.; Yong, K. Enhancing Stability of Perovskite Solar Cells to Moisture by the Facile Hydrophobic Passivation. *ACS Appl. Mater. Interfaces* **2015**, *7*, 17330−17336.

(16) Hwang, K.; Jung, Y.-S.; Heo, Y.-J.; Scholes, F. H.; Watkins, S. E.; Subbiah, J.; Jones, D. J.; Kim, D.-Y.; Vak, D. Toward Large Scale Roll-to-Roll Production of Fully Printed Perovskite Solar Cells. *Adv. Mater.* **2015**, *27*, 1241−1247.

(17) Mei, A.; Li, X.; Liu, L.; Ku, Z.; Liu, T.; Rong, Y.; Xu, M.; Hu, M.; Chen, J.; Yang, Y.; Grätzel, M.; Han, H. A Hole-Conductor−free, Fully Printable Mesoscopic Perovskite Solar Cell with High Stability. *Science* **2014**, *345*, 295−298.

(18) Schmidt, T. M.; Larsen-Olsen, T. T.; Carlé, J. E.; Angmo, D.; Krebs, F. C. Upscaling of Perovskite Solar Cells: Fully Ambient Roll Processing of Flexible Perovskite Solar Cells with Printed Back Electrodes. *Adv. Energy Mater.* **2015**, DOI: 10.1002/aenm.201500569.

(19) Yang, Z.; Chueh, C.-C.; Zuo, F.; Kim, J. H.; Liang, P.-W.; Jen, A. K.-Y. High-Performance Fully Printable Perovskite Solar Cells *via* Blade-Coating Technique under the Ambient Condition. *Adv. Energy Mater.* **2015**, DOI: 10.1002/aenm.201500328.

(20) Li, J.; Bade, S. G. R.; Shan, X.; Yu, Z. Single-Layer Light-Emitting Diodes Using Organometal Halide Perovskite/Poly(ethylene Oxide) Composite Thin Films. *Adv. Mater.* **2015**, *27*, 5196−5202.

(21) Kim, Y.-H.; Cho, H.; Heo, J. H.; Kim, T.-S.; Myoung, N.; Lee, C.-L.; Im, S. H.; Lee, T.-W. Multicolored Organic/Inorganic Hybrid Perovskite Light-Emitting Diodes. *Adv. Mater.* **2015**, *27*, 1248−1254.

(22) Li, G.; Tan, Z.-K.; Di, D.; Lai, M. L.; Jiang, L.; Lim, J. H.-W.; Friend, R. H.; Greenham, N. C. Efficient Light-Emitting Diodes Based on Nanocrystalline Perovskite in a Dielectric Polymer Matrix. *Nano Lett.* **2015**, *15*, 2640−2644.

(23) You, J.; Yang, Y. (M.); Hong, Z.; Song, T.-B.; Meng, L.; Liu, Y.; Jiang, C.; Zhou, H.; Chang, W.-H.; Li, G.; Yang, Y. Moisture Assisted Perovskite Film Growth for High Performance Solar Cells. *Appl. Phys. Lett.* **2014**, *105*, 183902.

(24) Eperon, G. E.; Habisreutinger, S. N.; Leijtens, T.; Bruijnaers, B. J.; van Franeker, J. J.; deQuilettes, D. W.; Pathak, S.; Sutton, R. J.; Grancini, G.; Ginger, D. S.; Janssen, R. A. J.; Petrozza, A.; Snaith, H. J. The Importance of Moisture in Hybrid Lead Halide Perovskite Thin Film Fabrication. *ACS Nano* **2015**, *9*, 9380−9393.

(25) Bass, K. K.; McAnally, R. E.; Zhou, S.; Djurovich, P. I.; Thompson, M. E.; Melot, B. C. Influence of Moisture on the Preparation, Crystal Structure, and Photophysical Properties of Organohalide Perovskites. *Chem. Commun.* **2014**, *50*, 15819−15822.

(26) Shi, D.; Adinolfi, V.; Comin, R.; Yuan, M.; Alarousu, E.; Buin, A.; Chen, Y.; Hoogland, S.; Rothenberger, A.; Katsiev, K.; Losovyj, Y.; Zhang, X.; Dowben, P. A.; Mohammed, O. F.; Sargent, E. H.; Bakr, O. M. Low Trap-State Density and Long Carrier Diffusion in Organolead Trihalide Perovskite Single Crystals. *Science* **2015**, *347*, 519−522.

(27) Christians, J. A.; Miranda Herrera, P. A.; Kamat, P. V. Transformation of the Excited State and Photovoltaic Efficiency of CH3NH3PbI3 Perovskite upon Controlled Exposure to Humidified Air. *J. Am. Chem. Soc.* **2015**, *137*, 1530−1538.

(28) Hoye, R. L. Z.; Chua, M. R.; Musselman, K. P.; Li, G.; Lai, M.-L.; Tan, Z.-K.; Greenham, N. C.; MacManus-Driscoll, J. L.; Friend, R. H.; Credgington, D. Enhanced Performance in Fluorene-Free Organometal Halide Perovskite Light-Emitting Diodes Using Tunable, Low Electron Affinity Oxide Electron Injectors. *Adv. Mater.* **2015**, *27*, 1414−1419.

(29) Aygüler, M. F.; Weber, M. D.; Puscher, B. M. D.; Medina, D. D.; Docampo, P.; Costa, R. D. Light-Emitting Electrochemical Cells Based on Hybrid Lead Halide Perovskite Nanoparticles. *J. Phys. Chem. C* **2015**, *119*, 12047−12054.

(30) Yu, J. C.; Kim, D. B.; Baek, G.; Lee, B. R.; Jung, E. D.; Lee, S.; Chu, J. H.; Lee, D.; Choi, K. J.; Cho, S.; Song, M. H. High-Performance Planar Perovskite Optoelectronic Devices: A Morpho-




DOI: 10.1021/acsnano.5b07506
*ACS Nano* 2016, 10, 1795−1801

logical and Interfacial Control by Polar Solvent Treatment. *Adv. Mater.* **2015**, *27*, 3492−3500.
(31) Yu, Z.; Niu, X.; Liu, Z.; Pei, Q. Intrinsically Stretchable Polymer Light-Emitting Devices Using Carbon Nanotube-Polymer Composite Electrodes. *Adv. Mater.* **2011**, *23*, 3989−3994.



DOI: 10.1021/acsnano.5b07506
*ACS Nano* 2016, 10, 1795−1801